OXFORD

GENERAL ARTICLE

FOXO1 controls protein synthesis and transcript abundance of mutant polyglutamine proteins, preventing protein aggregation

Gabriel Vasata Furtado[1],[†], Jing Yang[1],[†], Di Wu[1],[†],
Christos I. Papagiannopoulos[1], Hanna M. Terpstra[1], E. F. Elsiena Kuiper[1],
Sybille Krauss[2], Wei-Guo Zhu[3], Harm H. Kampinga[1],[‡] and Steven Bergink[1],[‡]*

[1]Department of Biomedical Sciences of Cells and Systems, University Medical Center Groningen, University of Groningen, Antonius Deusinglaan 1, Groningen 9713 AV, The Netherlands, [2]Faculty IV: School of Science and Technology, Institute of Biology, Human Biology / Neurobiology, University of Siegen, Adolf-Reichwein-Str. 2, 57076 Siegen, Germany and [3]Department of Biochemistry and Molecular Biology, Shenzhen University School of Medicine, Nanshan District, 1066 Xueyuan Avenue, Shenzhen 508055, China

*To whom correspondence should be addressed at. Tel: +31 503616111; Email: s.bergink@umcg.nl

Abstract

FOXO1, a transcription factor downstream of the insulin/insulin like growth factor axis, has been linked to protein degradation. Elevated expression of FOXO orthologs can also prevent the aggregation of cytosine adenine guanine (CAG)-repeat disease causing polyglutamine (polyQ) proteins but whether FOXO1 targets mutant proteins for degradation is unclear. Here, we show that increased expression of FOXO1 prevents toxic polyQ aggregation in human cells while reducing FOXO1 levels has the opposite effect and accelerates it. Although FOXO1 indeed stimulates autophagy, its effect on polyQ aggregation is independent of autophagy, ubiquitin–proteasome system (UPS) mediated protein degradation and is not due to a change in mutant polyQ protein turnover. Instead, FOXO1 specifically downregulates protein synthesis rates from expanded pathogenic CAG repeat transcripts. FOXO1 orchestrates a change in the composition of proteins that occupy mutant expanded CAG transcripts, including the recruitment of IGF2BP3. This mRNA binding protein enables a FOXO1 driven decrease in pathogenic expanded CAG transcript- and protein levels, thereby reducing the initiation of amyloidogenesis. Our data thus demonstrate that FOXO1 not only preserves protein homeostasis at multiple levels, but also reduces the accumulation of aberrant RNA species that may co-contribute to the toxicity in CAG-repeat diseases.

Introduction

The expansion of cytosine adenine guanine (CAG) repeats in at least 9 different genes causes neuronal dysfunction and degeneration leading to Huntington's disease, dentatorubral–pallidoluysian atrophy, spinal and bulbar muscular atrophy, spinocerebellar ataxias type 1, 2, 3, 6, 7 and 17 (1,2). These CAG expansions encode for glutamine (Q) and the polyglutamine

---

(polyQ) expanded proteins have a high tendency to form toxic amyloidogenic aggregates (1–5). These aggregates reflect a loss in protein homeostasis that underlies many neurodegenerative diseases including the CAG expansion diseases or so-called polyglutaminopathies (3,4). Protein homeostasis entails the balance between protein synthesis, folding and degradation (6). The importance of maintaining protein homeostasis is further strengthened by the notion that several proteins that function in preserving protein homeostasis can prevent or resolve protein aggregation and delay onset of disease in various model systems (4). Next to the formation of toxic protein aggregates, the expansion of CAG repeats also affects the structure of the mutant transcript which also may contribute to neuronal degeneration (7,8).

Similar to all other neurodegenerative diseases, there is currently no cure or treatment that can effectively delay symptoms of the polyglutaminopathies. Several targets and strategies have been identified that can delay aggregate formation (9–12). One of these is the Insulin/Insulin like growth hormone (IGF) axis and its downstream transcription factor families heat shock factor (HSF) and Forkhead box O (FOXO) (13–19). Elevated expression of DAF-16 (the homolog of FOXO in *Caenorhabditis elegans*) is sufficient to reduce protein aggregation and is associated with life span extension as well (20,21).

Here, we show that FOXO1 effectively reduces polyQ aggregation in human cells and that this is mediated via a reduction in the steady-state levels of mutant polyQ proteins, whereas proteins with a normal Q length are unaffected. Surprisingly, this reduction is independent of autophagy, ubiquitin–proteasome system (UPS) mediated protein degradation and is not due to a change in mutant polyQ protein turnover in general. Instead, elevated FOXO1 levels specifically reduce the synthesis of polyQ proteins with pathological Q lengths. This decrease in protein synthesis is dependent on the RNA binding proteins DDX18, IGF2BP3 and STAU1. Furthermore, FOXO1 affects the mRNA stability of expanded CAG constructs in an IGF2BP3-dependent manner. FOXO1 thus acts on polyQ encoding transcripts by recruiting RNA binding proteins resulting in reduced transcript levels and mutant protein synthesis.

Results

To test whether FOXO1 can reduce the aggregation of polyQ proteins in human cells, we used a GFP tagged exon1 fragment of the human Huntingtin protein with an expanded polyQ track (HTT^{Q43}GFP). Co-expression of FLAG-tagged FOXO1 (Flag-FOXO1) strongly reduced HTT^{Q43}GFP retention of polyQ aggregates in a filter trap assay (FTA) (Fig. 1A), a method that captures aggregates by size using a cellulose acetate filter with 200 nm pores (22). This suppressive effect of Flag-FOXO1 on HTT^{polyQ} aggregation is independent of the GFP tag as similar results were obtained using HA-HTT^{Q43} (Fig. 1B). Moreover, Flag-FOXO1 reduced the aggregation of HTT^{polyQ} constructs with significantly longer polyQ tracts, HTT^{Q71}GFP and HTT^{Q119}YFP as well (Fig. 1C and D). As an alternative method to measure aggregation we used HTT^{Q119}YFP induced puncta formation which was reduced as well by co-expression of Flag-FOXO1 (Fig. 1E and F) in line with previous findings (23). Remarkably, the effect of Flag-FOXO1 is not restricted to the aggregated fraction but also lowered the amount of mutant protein in the soluble fraction (Fig. 1G and H). This reduction in HTT^{polyQ} protein level is specific to mutant polyQ proteins as levels of GFP alone did not change upon Flag-FOXO1 expression (Fig. 1I). Inversely, reducing FOXO1 levels using siRNA enhanced polyQ aggregation. Thus,

increasing FOXO1 levels reduces polyQ aggregation, whereas decreasing FOXO1 has the opposite effect and accelerates polyQ aggregation. Together, these data show that the levels of FOXO1 are a key determinant of polyQ aggregation.

FOXO1 is a transcription factor containing a DNA binding domain (DBD) and transcription activation domain (TAD) (Fig. 2A). Both domains are required for the reduction in both soluble HA-HTT^{Q43} protein and aggregates (Fig. 2B and C), suggesting that the effects of FOXO1 are related to its transcriptional activity. Several proteins involved in protein quality control have been suggested as downstream targets of the transcriptional activity of FOXO. Among these targets are so-called small heat shock proteins (HSPBs) (21) some of which are known to reduce polyQ aggregation, in particular HSPB7 (24,25). Of the nine HSPBs that we tested, HSPB2, HSPB4, HSPB5 and HSPB6 were indeed moderately upregulated upon FOXO1 expression, while HSPB7 was not (Fig. 2D). However, when ectopically overexpressed, neither HSPB2, HSPB4, HSPB5 nor HSPB6 could reduce polyQ aggregation (24). Moreover, the Flag-FOXO1 mediated transcriptional upregulation did not result in a detectable increase in the protein levels of these HSPBs (Fig. 2E). These results argue against a FOXO1-mediated role of HSPBs in reducing polyQ aggregation.

Rather than by a pathway of chaperone-assisted protein degradation, FOXO/DAF-16 has been suggested to more directly control protein degradation via activating autophagy or the UPS (26–28). Flag-FOXO1 expression indeed induced autophagy (Supplementary Material, Fig. S1A) and the inhibition of autophagy using a chemical cocktail of E64, pepstatin A and bafilomycin A1 enhanced the levels of polyQ aggregates (Fig. 3A) in line with previous results (28,29). However, autophagy inhibition did not affect the Flag-FOXO1 mediated reduction of neither polyQ aggregates (Fig. 3A) nor soluble protein (Fig. 3B). Macroautophagy defective ATG5−/− mouse embryonic fibroblast (MEF) (30), showed similar results: overexpression of Flag-FOXO1 reduced polyQ aggregation to a similar level as in wild-type (WT) control cells (Fig. 3C). Autophagy-dependent processes are blocked in the ATG5−/− MEFs exemplified by the inability to form lipidated LCR (LCR II, Fig. 3C). To even further ensure that degradation of substrates like HTT^{polyQ} via autophagy is truly blocked in the ATG5−/− cells, we tested the effect of BAG3. BAG3 is a co-chaperone that induces autophagy and reduces polyQ aggregation in an autophagy-dependent manner (31). Although BAG3 reduced HA-HTT^{Q43} aggregation in WT cells, it did not reduce in the ATG5−/− cells (Fig. 3C). Finally, in human cells effects of FOXO1 on autophagy have been shown to be independent of its DBD (28), whereas we found that both the DBD and TAD were required for its effects on polyQ proteins (Fig. 2B and C).

Next, we tested whether canonical degradation via the UPS is involved in the aggregate-reducing activity of FOXO1. Blocking the UPS by either MG132 or bortezomib resulted in a typical increase in polyubiquitylated material (Fig. 3D). Despite this block of UPS-dependent degradation, Flag-FOXO1 expression still reduced the protein level of HA-HTT^{Q43} and HTT^{Q71}GFP (Figs 3D and Supplementary Material, Fig. S1B) and the amount of aggregates as well (Figs 3E and Supplementary Material, Fig. S1C).

To rule out the involvement of rare proteases or other protein degradation activities, we used pulse chase with heavy isotope labelling experiments to assess whether FOXO1 affects protein turnover of polyQ proteins. HTT^{polyQ} constructs are remarkably long lived and Flag-FOXO1 expression did not influence this
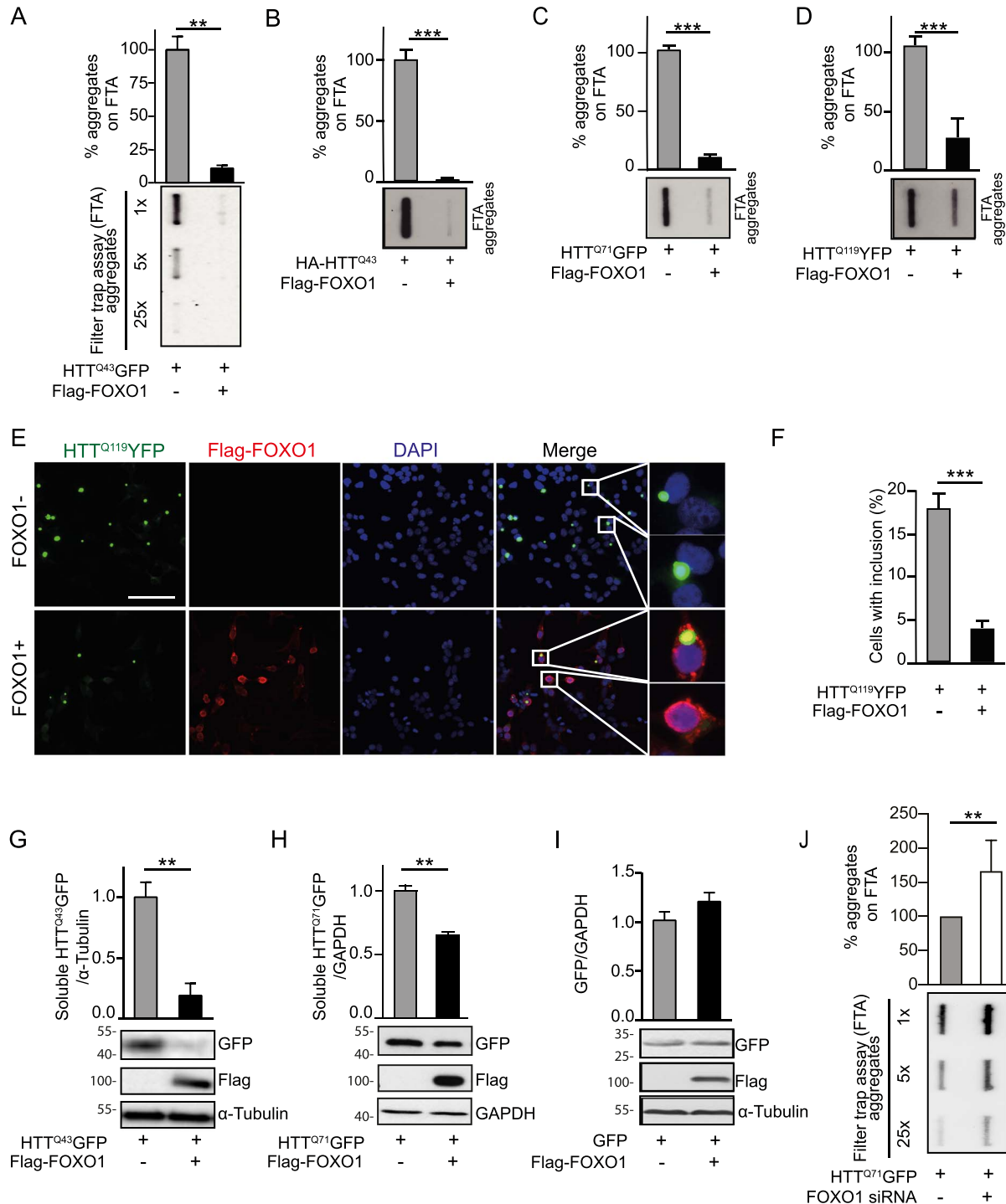
Figure 1. FOXO1 reduces mutant HTT aggregation. (**A–D**) Filter trap analysis of different mutant HTT constructs in presence or absence of Flag-FOXO1. HEK293T cells expressing HTT^{Q43}GFP, HA-HTT^{Q43}, HTT^{Q71}GFP or HTT^{Q119}YFP with (black bar) or without (grey bar) Flag-FOXO1. Insoluble HTT^{Q43}GFP (A) HA-HTT^{Q43} (B), HTT^{Q71}GFP (C) or HTT^{Q119}YFP (D) aggregation was detected by filter trap and quantified. Lower panels depict filter trap blots probed with GFP antibody. Upper panel shows a graph that depicts the mean and standard error of mean (SEM) of 3 replicates. P-values were derived from two-tailed Student's t test. (**E**) Representative IF staining of HEK293T cells co-expressing HTT^{Q119}YFP with or without Flag-FOXO1 (lower and upper row). First column depicts HTT^{Q119}YFP (green), the second column depicts Flag-FOXO (red), the third column depicts DAPI (in blue) and the fourth column shows the merge. Inlay depicts the localization of Flag-FOXO in relation to the nucleus. Bar = 100 μm. (**F**) Quantification of cells treated as in E. Graph showing the mean and standard deviation (SD) of three independent replicates. (**G–I**) Western blot analysis of HEK293T cells expressing HTT^{Q43}GFP (G), HTT^{Q71}GFP (H) or GFP (I) is shown. Lower panels western blots using the indicated antibodies are shown. Upper panels graphs depicting the mean and SD of 3 independent experiments is shown. All panels, P-values were derived from two-tailed Student's t test. (**J**) Filter trap analysis of HEK293 cells expressing HTT^{Q71}GFP, treated with the indicated siRNA. Lower panels depict filter trap blots probed with GFP antibody. Upper panel shows a graph that depicts the mean and SEM of 4 replicates.
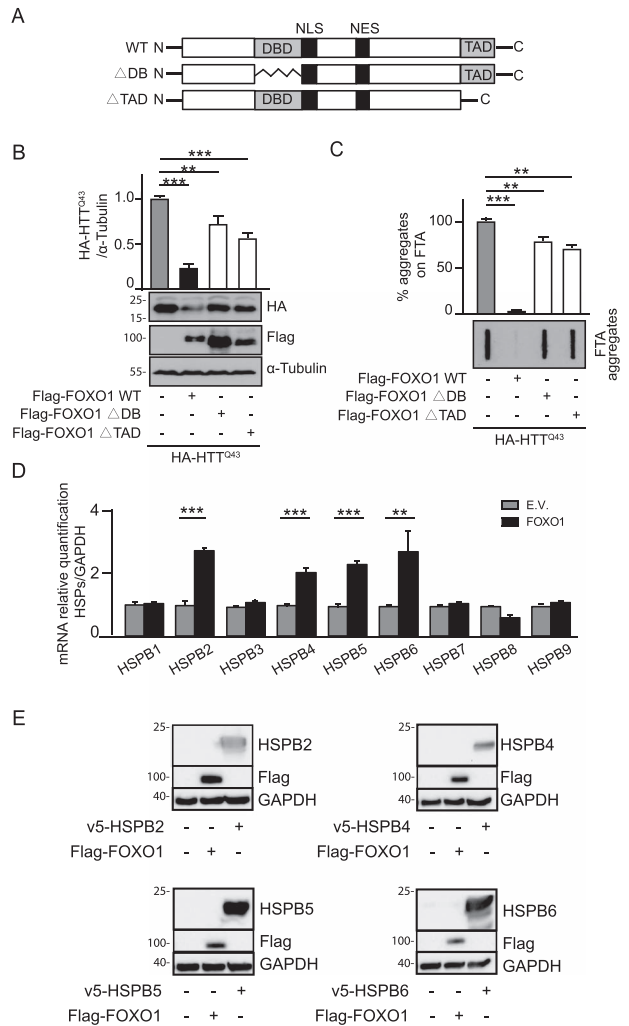
Figure 2. HSPBs protein expression is not significantly changed by FOXO1. (**A**) Schematic representation of FOXO1 and truncation mutants used. (**B**) Western blot analysis of cells expressing HA-HTT^{Q43} (grey bar) and Flag-FOXO1 (black bar) or its truncated mutants (white bars). Lower panel depicts immunoblots against the indicated antibodies. Upper panel graph depicts the mean and SEM of 3 independent experiments. (**C**) Filter trap analysis of cells treated as in B. Lower panel filter trap probed with HA antibody is shown. Upper panel graph depicts the mean and SEM of 3 independent experiments. **$P < 0.001$; ***$P < 0.0001$. (**D**) qPCR analysis of HEK293T cells transfected with (black bars) or without (grey bars) Flag-FOXO1. Graph depicts the relative levels of the indicated genes. All data were normalized to GAPDH and were corrected to EV. (**E**) Analysis of protein expression levels induced by Flag-FOXO1 expression. HEK293T cells were transfected with EV, Flag-FOXO1 or a V5 tagged HSPB (as an antibody control). Representative western blots using antibodies against HSPB2, HSPB4, HSPB5, HSPB6, Flag and GAPDH are shown. **$P < 0.001$; ***$P < 0.0001$.

(Fig. 3F and G), showing that FOXO1 reduces protein levels independent of an activity that accelerates protein turnover.

Because steady-state levels were lower and degradation was unaffected in conditions of Flag-FOXO1 expression, we argued that maybe protein synthesis could be affected and determined the synthesis rate of HTT^{Q43}GFP in the presence or absence of Flag-FOXO1. Using pulse labelling with heavy isotope labelled methionine and cysteine we noted a strong drop in newly synthesized HTT^{Q43}GFP protein in the presence of Flag-FOXO1, demonstrating that Flag-FOXO1 reduces HTT^{Q43}GFP protein synthesis (Fig. 4A and B). Importantly, Flag-FOXO1 expression

did not affect total protein synthesis, arguing that this effect is specific (Supplementary Material, Fig. S2A and B). Flag-FOXO1 still reduced polyQ aggregates after depletion of the ribosome-associated E3 ligase Ltn1 (Supplementary Material, Fig. S2C). This speaks against a role of ribosomal protein quality control (32) and is in line with our results that the drop in steady-state level is independent of protein degradation. Instead, we noted a strong reduction in the mRNA levels of various expanded polyQ constructs (Figs 4C and Supplementary Material, Fig. S2D). This Flag-FOXO1-mediated drop in mRNA is specific to pathogenic expansion as neither GFP nor HTT^{CAG25}GFP mRNA levels dropped in the presence of Flag-FOXO1 (Figs 4C and Supplementary Material, Fig. S2D). Similarly, the mRNA levels of the endogenous (non-expanded) 'Huntingtin' gene remained the same in the presence of Flag-FOXO1 overexpression (Figs 4D and Supplementary Material, Fig. S2E). In summary, elevated levels of Flag-FOXO1 specifically reduce expanded polyQ (i.e. CAG) mRNA levels.

Expansion of CAG in the alleles of patients who suffer from polyglutaminopathies not only leads to toxic proteins with long polyQ tracts, but also results in an altered mRNA structure (8). The expansion of CAG in the disease-causing alleles severely impacts the 3D folding of the transcribed mRNA (HTT^{polyCAG}) and forms a double hairpin (7). This altered structure results in differential binding of RNA-binding proteins (RBPs) (33–36). To test whether expression of Flag-FOXO1 altered the composition of proteins that bind to HTT^{polyCAG}-mRNA, we performed pull downs with *in vitro* transcribed biotinylated HTT^{CAG47}-mRNA as bait in cells expressing Flag-FOXO1 or not (Supplementary Material, Fig. S3A). Bioinformatic analysis of the identified hits revealed that mRNA processing and translation initiation factors as GO terms were reduced in cells expressing Flag-FOXO1, whereas mRNA binding was enriched (Fig. 5A). In total, we identified 23 proteins that were unique in HTT^{CAG47} binding in cells that express Flag-FOXO1 including FOXO1 itself (Supplementary Material, Fig. S3B). Six of these proteins, STAU1, IGF2BP3, FUS, DDX18, DDX41 and TAF15, were predicted to bind to RNA (DAVID 6.8 database, Supplementary Material, Fig. S3C). Next, we tested whether the expression of FOXO1 or HTT^{Q71}GFP had an impact on the transcriptional regulation of these putative RBPs. Elevated expression of Flag-FOXO1 alone did not significantly impact the transcription of any of these genes (Fig. 5B). Instead, Flag-FOXO1 expression reverted the increase in mRNA of STAU1, IGF2BP3 and DDX41 after HTT^{Q71}GFP expression (Fig. 5B), whereas DDX18 was transcriptionally upregulated only in the presence of both Flag-FOXO1 and HTT^{Q71}-GFP (Fig. 5B). We also noted that three of these six proteins, namely IGF2BP3, DDX18 and DDX41, are part of so-called processing bodies (p-bodies) (37). This is interesting as several mRNA turnover and silencing processes take place in p-bodies (38). Elevated levels of FOXO1 increased the number and size of p-bodies in both HTT^{Q25}GFP as HTT^{Q71}GFP expressing cells (Fig. 5C–E). This indicates that FOXO1 is important for stimulating p-body formation.

Of the six RBPs that were enriched in binding to HTT^{CAG47}-mRNA in the presence of Flag-FOXO1, CRISPRi-mediated knockdown (39) of either STAU1, IGF2BP3 or DDX18 ablated the anti-polyQ aggregation effect of Flag-FOXO1 on HTT^{Q71}GFP (Fig. 5F), whereas FUS, DDX41 and TAF15 knockdown had no effect (Supplementary Material, Fig. S3D). Interestingly, IGF2BP3 knockdown reverted the drop in HTT^{CAG71}-GFP mRNA in a Flag-FOXO1 overexpression background, whereas STAU1 and DDX18 knockdown did not (Figs 5G and Supplementary Material, Fig. S3E). Thus, FOXO1 expression results in a decrease in synthesis of polyQ proteins, this reduced synthesis is explained by a specific drop
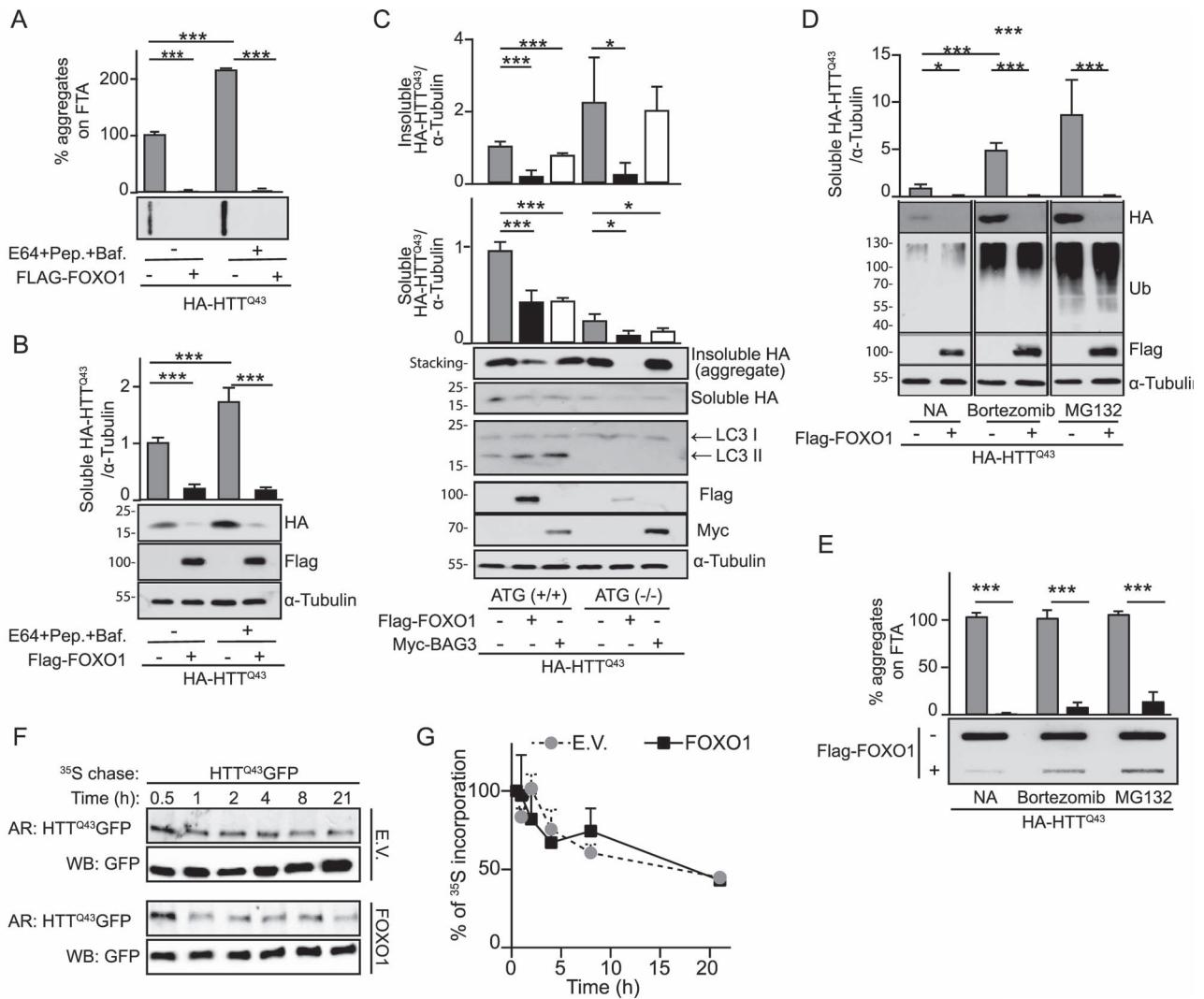
Figure 3. The effects of FOXO1 on mutant HTT aggregation are unrelated to protein degradation. (**A**) FTA of HEK293T cells expressing HA-HTT^{Q43} with or without Flag-FOXO1 and treated with autophagy inhibitors or not. Autophagy inhibitors were added 18 h after transfection. Lower panel depicts a filter trap blot probed with HA antibodies. Upper panel depicts the graph with the quantification. Mean and SEM of three independent experiments are shown. (**B**) Western blot analysis of HEK293T cells receiving the same treatment as in A. Lower panel: western blots using the indicated antibodies are shown. Upper panel: graph with quantification of soluble HA signal normalized against α-tubulin is shown. Mean and SEM of three independent experiments are shown. (**C**) Protein fractionation analysis of Atg5 (+/+) and Atg5 (−/−) MEFs expressing HA-HTT^{Q43} with (black bar) or without (grey bar) Flag-FOXO1, or MYC-BAG3 (white bar). Lower panel: soluble and insoluble HA-HTT^{Q43} were detected by western blotting using the indicated antibodies. Upper panels graphs depicting the quantification of insoluble (up) or soluble (below) HA-HTT^{Q43}. The mean and SEM of 3 independent experiments are shown. (**D**) Western blot analysis of HEK293T cells expressing HA-HTT^{Q43} with or without FOXO1, followed by proteasome inhibitor treatments (Bortezomib or MG132) for 6 h. Lower panel a filter trap probed against HA antibodies is shown. Upper panel depicts the graph with the Mean and SEM of three independent experiments. (**E**) Filter trap analysis of cells treated as in D. Lower panel, western blots using the indicated antibodies are shown. Upper panel, graph depicting the mean and SEM of three independent experiments is shown. (**F**) Pulse chase analysis of HTT^{Q43}GFP. HEK293T cells expressing HTT^{Q43}GFP with or without Flag-FOXO1 were pulse labelled with cys/met-35S for 40 min followed by a cold chase for the indicated time. At each time point cells were lysed and HTT^{Q43}GFP was immunoprecipitated using GFP-trap®. Autoradiography (AR indicating the 35S signal) and western blot using GFP are shown. EV stands for empty vector. The data of the control (EV) have been published before as these experiments were conducted together (10). (**G**) Quantification of percentage of 35S incorporated in HTT^{Q43}GFP with (black squares) or without (grey circle) FOXO1 over time, normalized to total GFP and to time point 0.5 h. The mean and SEM of 3 independent experiments are shown. All panels: P-values were derived from two-tailed Student's t test. *$P < 0.05$; ***$P < 0.0001$.

in mRNA abundance of expanded polyQ (CAG) and depends on the putative RBP IGF2BP3.

Discussion

Here we show that the level of expression of FOXO1 is a key determinant in the extent of polyQ aggregation. Elevated expression of FOXO1 efficiently reduces the level of soluble and aggregated polyQ-containing proteins, whereas depletion of FOXO1 accelerates polyQ aggregation. Increased levels of FOXO1 have been associated with an increased autophagic flux (28), something we observe as well. Although we do not exclude a minor role for autophagy, we find that the effects of FOXO1 expression on polyQ aggregation are largely independent of protein degradation in general. Instead, we show that FOXO1 expression results in a specific decrease in synthesis of polyQ proteins with pathologically expanded repeats. This reduced synthesis is explained by a drop in mRNA abundance of
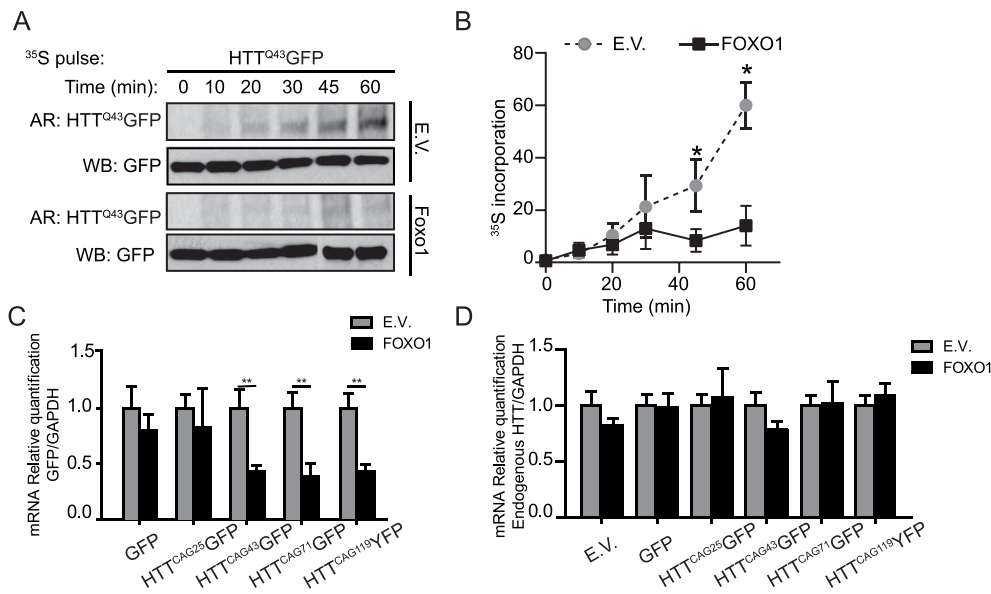
Figure 4. FOXO1 specifically reduces mRNA levels of HTT transcripts with pathological CAG length. (**A**) Pulse labelling analysis of HTT^{Q43}GFP. HEK293T cells expressing HTT^{Q43}GFP with or without Flag-FOXO1 were pulse labelled with cys/met-35S for the indicated times. At each time point cells were lysed and HTT^{Q43}GFP was immunoprecipitated using GFP-trap$^{\circledR}$. AR (AR indicating the 35S signal) and western blot using GFP are shown. EV stands for empty vector. The data of the control (EV) have been published before as these experiments were conducted together (García-Huerta *et al.* 2020). (**B**) Quantification of pulse labelling in A. Graph depicts the percentage of 35S incorporated over times in HTT^{Q43}GFP with (black squares) or without (grey circle) expression of Flag-FOXO1, normalized to total GFP and to time point zero. Mean and SEM of 3 independent experiments are shown. (**C**) qPCR analysis of HEK293T cells expressing different HTT^{CAG} sizes with (black bars) or without (grey bars) Flag-FOXO1 using primers detecting GFP. All data were normalized to GAPDH and were corrected to EV Graph depicting the mean and SEM of 3 independent experiments is shown. All panels: P-values were derived from two-tailed Student's t test. (**D**) Relative quantification of endogenous HTT$^{CAGnon-expanded}$ expression with (black bars) or without (grey bars) Flag-FOXO1 and different sizes of exogenous HTT^{CAG} by qPCR. All data were normalized by GAPDH as reference and were corrected to EV All images show typical experiments; all experiments were repeated three times. P-values were derived from two-tailed Student's t test. *P < 0.05; **P < 0.001; ***P < 0.0001.

expanded polyQ (CAG) alleles and depends on the putative mRNA binding protein IGF2BP3. Importantly IGF2BP3 binds to HTT^{polyCAG}-mRNA and this is enhanced by FOXO1 expression.

It is intriguing that the regulation of pathogenic polyQ levels occurs at the transcript level. The requirement of the nucleotide binding domain (the DBD) may speak for a transcriptional role of FOXO1 in suppressing polyQ aggregation (Fig. 2). However, we did not identify an obvious pattern in the transcriptional activation after FOXO1 expression of the polyQ mRNA binding proteins that we tested (Fig. 5B). Moreover, in our IF experiments (Fig. 1E), we did not observe a clear recruitment of FOXO1 to the nucleus. Instead, FOXO1 expression facilitates a change in the composition of the proteins bound to the poly-CAG mRNA. This change leads to mRNA silencing and decay activities. The upregulation of p-bodies—a hub for various RNA related processes including mRNA decay and silencing (38)—after FOXO1 expression argues that FOXO1 may have a similar impact on other (perhaps mutant) mRNAs as well.

FOXO1 effectively decreases the translation of polyQ proteins and mediates a change in the mRNA-protein complex composition of expanded CAG constructs. On the one hand, this results in a drop in ribosome occupancy on HTT^{polyCAG}-mRNA, very much in line with the reduced synthesis of polyQ proteins upon FOXO1 expression. On the other hand, several mRNA binding proteins display a preference for HTT^{polyCAG}-mRNA in the presence of FOXO1. Of these, STAU1, DDX18 and IGF2BP3 are required for the drop in polyQ aggregates.

In contrast to STAU1 and DDX18, IGF2BP3 is required for both the reduced polyQ aggregation and the drop in polyCAG mRNA that are triggered by FOXO1 expression. In several tumours, IGF2BP3 is upregulated and results in an increase (and not a decrease) in the mRNA stability of numerous oncogenes (40).

IGF2BP3 also triggers the interaction of transcripts with the RNA-induced silencing complex (RISC) (41), which is central in the regulation of transcript abundance and facilitates both silencing (translation blockage) as well as mRNA decay (42). RISC components have been identified as part of p-bodies (37). The IGF2BP3-dependent effects of FOXO1 on polyCAG transcript abundance have a remarkable overlap with the role of RISC. Also, their shared link with p-bodies suggests an interplay between FOXO1 and RISC. Interestingly, in *C. elegans* the longevity phenotype of Argonaut mutants (a RISC constituent) depends on FOXO (43).

Next to the recruitment of STAU1, DDX18, IGF2BP3, FUS, DDX41 and TAF15, it is noteworthy that we also picked up FOXO1 as a putative polyQ mRNA binding protein. Currently, it is unclear whether FOXO1 can bind to RNA and if this plays a role in the effects we observed here.

Insulin signalling has been long suggested as capable of restoring protein homeostasis in protein aggregation diseases (11,13,15,17,18). Although the downstream transcription factor family HSF has extensively been investigated from invertebrates to mammals for its efficacy in protein aggregation diseases, the potential of the FOXO family has so far been investigated almost exclusively in invertebrates. Here, we show that this potential of FOXO1 extents to mammalian cells, implying that FOXO1 could be an excellent target for therapy against polyglutaminopathies. FOXO1 decreases the abundance of expanded CAG transcripts and hence the load of mutant protein. FOXO1 could thus be considered as a valuable adjuvant in the anti-sense lowering strategies that are currently tested in phase III trials (44). Moreover, on top of its primary action on polyQ transcript abundance, the FOXO-regulated upregulation of autophagy may provide the second ring of protection against polyQ aggregation. This may
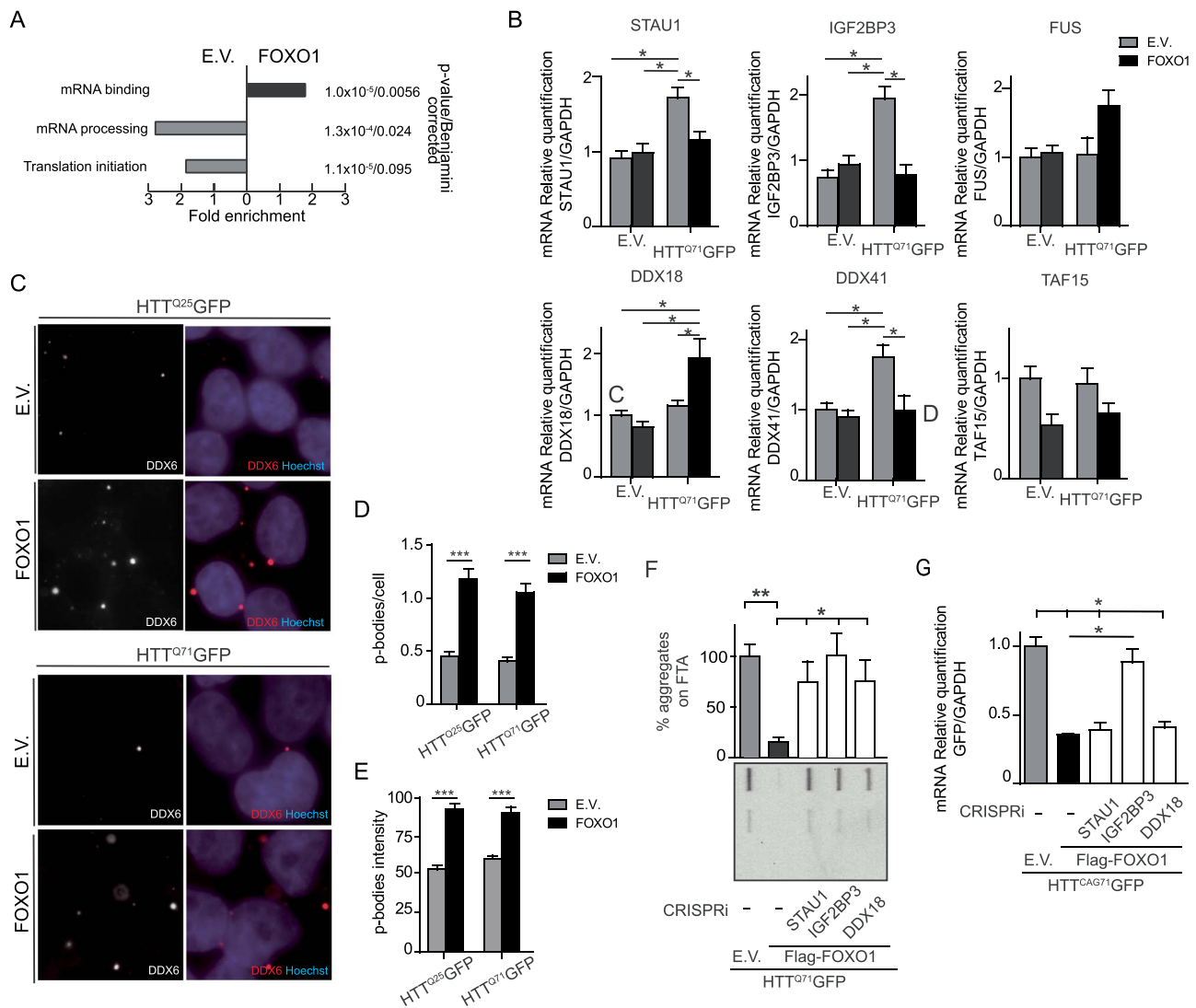
Figure 5. FOXO1 requires mRNA binding proteins to affect polyQ levels. (**A**) GO analysis (using DAVID 6.8) of proteins bound to GFP-HTT^{CAG47} mRNA with (black bars) or without (grey bars) Flag-FOXO1 overexpression. (**B**) qPCR analysis of STAU1, IGF2BP3, FUS, DDX18, DDX41 and TAF15 in cells that express Flag-FOXO1 or not, and in presence or absence of HTT^{Q71}GFP. All data were normalized to GAPDH as reference and were corrected to EV. (**C**) Representative immunofluorescence pictures detecting p-bodies (using DDX6 antibodies). HEK293T cells expressing HTT^{Q25}GFP (Left panel) or HTT^{Q71}GFP (Right panel) with and without Flag-FOXO1 (lower and upper row) were stained with a DDX6 antibody (red). Nucleus stained with Hoechst (blue). (**D**) Graph depicting quantification of the number of p-bodies per cell of cells treated as in C. (**E**) Graph depicting p-bodies intensity of cells treated as in C. (D and E) Mean and SEM of three independent experiments are shown. *P*-values were derived from two-tailed Student's t test. (**F**) Filter trap analysis of cells expressing HTT^{Q71}GFP, Flag-FOXO1 (or not) after knock down of STAU1, IGF2BP3 or DDX18 using CRISPRi. Lower panel depicts a filter trap probed with GFP antibodies. Upper panel depicts the graph with the mean and SEM of three independent experiments. (**G**) qPCR analysis of cells treated as in F. Relative quantification of HTT^{CAG71}GFP mRNA expression normalized to GAPDH and corrected to EV. *P*-values were derived from 1 way analysis of variance with the Bonferroni correction. *$P < 0.05$; **$P < 0.001$; ***$P < 0.0001$

explain its high efficacy in combatting disease phenotypes in experimental invertebrate disease models and also imply that it has both disease preventive and disease therapeutic potential.

Materials and Methods

Cell culture and chemicals and reagents

HEK293T cell (ATCC) and MEF were cultured in Dulbecco's modified Eagle's medium (DMEM, Gibco) with 10% fetal calf serum (Greiner Bio-one, Longwood, FL, USA) in a 37°C incubator with 5% CO_2. Cells were transfected using Lipofectamine (Invitrogen) according to the manufacturer's instruction or using polyethylenimine (Invitrogen) following manufacturer's protocol. Bortezomib, MG132, E64, pepstatin A, Balfilomycin A 1 and cycloheximide were purchased from Sigma. siRNA against Ltn1

was bought from Ambion. siRNA against FOXO1 were obtained from Dharmacon and have been described previously (45).

DNA constructs

Full Huntingtin exon1 fragments (MATLE … KKDRV) with different polyQ lengths were cloned into p.EGFP vectors, either EGFP-C1 between NheI and BamHI sites or EGFP-N1 between BglII and BamHI sites. HA-HTT^{Q43} and HTT^{Q119}YFP (46), MYC-BAG3 (47). PCDNA3-FLAG-FOXO1 and truncation mutants (28) have been described previously.

The V5-FOXO1 fragment was amplified from PCDNA3-FLAG-FOXO1 construct with BamH1 and XhoI restriction sites on 5′ and 3′ terminal, respectively (The following primers were used: Forward: ATCTTGGATCCATGGGTAAGCCTATCCCTAACCCTCTC-CTCGGTCTCGATTCTACGGCCGAGGCGCCTCAGGTGGTGGAGATC,

Reverse: GATTACCTCGAGTCAGCCTGACACCCAGCTATGTGTCG-TTG); after digest; the fragment was inserted into the flip recombination target/*tet* operator2 (FRT/TO) vector. The construct was checked by sequencing.

Western blotting and FTA

Western blot and FTA analysis have been described previously (48). For western blot, cells were lysed in FTA sample buffer (10 mM Tris–HCl, 150 mM NaCl, 2% sodium dodecyl sulfate (SDS), pH = 8.0) and were boiled with an equal amount of $2\times$ Laemmli buffer. Samples were then loaded and run on a 12% SDS page gel and transferred (Bio-Rad). After transfer, membranes were blocked and incubated with primary and secondary antibodies followed by detection using the ChemiDoc Touch Imaging system (Bio-Rad). FTAs, 3.5×10^5 HEK293T cells were seeded on 6 well plates. Cells were lysed in 200 μL FTA sample buffer (10 mM Tris-Cl, pH 8.0, 150 mM NaCl, 2% SDS). Samples (100, 20 and 4 μg) were diluted in FTA sample buffer supplied with 50 mM dithiothreitol (DTT). Boiled samples were then applied onto a pre-washed (by FTA wash buffer, 10 mM Tris-Cl, pH 8.0, 150 mM NaCl, 0.1% SDS) 200 nm cellulose acetate filter (GE Water and Process Technologies, Trevose, PA, USA) with 2 Whattman papers (Bio-Rad, Hercules, CA, USA) in a Bio-Dot microfiltration apparatus (Bio-Rad). Gentle suction was applied to filtrate the samples followed by three times washing using FTA wash buffer. After blocking the membrane for 1 h in 10% milk, incubated with primary (overnight) and secondary antibodies (1 h), membrane was exposed using ChemiDoc Touch Imaging system (Bio-Rad).

Primary and secondary antibodies used: anti-GFP primary antibody (Invitrogen) at 1:5000 dilution; anti-HA primary antibody (abcam) at 1:1000 dilution; anti-Flag (sigma) at a 1:2000 dilution; anti-GAPDH primary antibody (Fitzgerald) at 1:10 000 dilution; anti-α-tubulin primary antibody (abcam) at 1:1000 dilution; anti-p62 primary antibody (Invitrogen) at a 1:2000 dilution; anti-LC3(CST) at a 1:2000 dilution; anti-HSPB2 primary antibody (abcam) at 1:1000 dilution; anti-HSPB4 primary antibody (StressMarq) at 1:1000 dilution; anti-HSPB5 primary antibody (StressMarq) at 1:1000 dilution; and anti-HSPB6 primary antibody (abcam) at 1:1000 dilution.

Immunofluorescence

Immunofluorescence (IF) was described previously (47). After transfection, cells grown on coverslips were fixed in 2% formaldehyde for 15 min, washed 2 times with phosphate buffered saline (PBS) and permeabilized with PBS-Triton X-100 (0.1%). Cells were washed with PBS and with PBS plus (PBS with 0.5% bovine serum albumin (BSA), 0.15% glycine), followed by primary antibody incubation overnight at 4°C. Cells on coverslips were washed with PBS plus for 4 times and were incubated with secondary antibody. After washing with PBS plus and PBS DNA was stained with DAPI or Hoechst (Thermo Fisher Scientific) for 5 min followed by washing with PBS. Cover slips were mounted in Vectashield (Agar Scientific). Mouse anti-v5 primary antibody (Invitrogen) at a 1:10 000 dilution, Rabbit anti-DDX6 primary antibody (Novus) at 1:1000, Alexa 594 anti-mouse (Invitrogen) secondary antibody was diluted as 1:1500, Alexa 633 anti-rabbit (Invitrogen) secondary antibody was diluted as 1:1000. Images were taken by a Leica sp8 confocal microscope and edited by Fiji.

RT-qPCR

Total RNA was isolated by RNA isolation kit (Stratagene) or by TRIZOL (Invitrogen) method followed by cDNA generating using Moloney murine leukaemia virus reverse transcriptase (Invitrogen). RT-qPCR was performed using SYBR green and iQ5 (Bio-Rad).

Primers for qPCR. GAPDH: F-TGCACCACCAACTGCTTAGC, R-GGCATGGACTGTGGTCATGAG;

HSPB1: F- ACGGTCAAGACCAAGGATGG, R- AGCGTGTATTTC-CGCGTGA;

HSPB2: F- ACCGCCGAGTACGAATTTG, R- GAGGCCGGA-CATAGTAGCCA;

HSPB3: F- ATAGAGATTCCAGTGCGTTACCA, R- CAGGCAGTG-CATATAAAGCATGA;

HSPB4: F- ACCGGGACAAGTTCGTCATC, R- CTCGTTGT-GCTTTCCGTGGAT;

HSPB5: F- AGGTGTTGGGAGATGTGATTGA, R- GGATGAAG-TAATGGTGAGAGGGT;

HSPB6: F- TGCTAGACGTGAAGCACTTCT, R- ACCACCTTGAC-AGCAATTTCC;

HSPB7: F- AAGGCCCTGAGCATGTTTTCC, R- ACTTGTGAGC-GAAGGTGTTCA;

HSPB8: F- CTCCTGCCACTACCCAAGC, R- GGCCAAGAGGCTGT-CAAGT;

HSPB9: F- ACCATGCCAGAGACGGTTTC, R- CATGCGGTAACT-GACCCTTTC;

GFP: F- ACGACGGCAACTACAAGACC, R- TTGTACTCCAGCTTGT-GCCC;

HA-HTT: F-CATACGACGTCCCAGACTAC,R- AATGATGATGAT-GATGATGCACGTGTAG;

EndogenousHTT: F-CCGCTCAGGTTCTGCTTTTAC, R- AGGA-CTTGAGGGACTCGAAGG;

STAU1: F- TCTCGGATGCAGTCCACCTA, R- GTGTTTCGCAGC-CTGTCTTG;

IGF2BP3: F- AGCTTTCTCGCTTTGCTGGA, R- GCCTTGAACT-GAGCCTCTGG;

FUS: F- GCTGGTGACTGGAAGTGTCC, R- TCATCCCCGTAGT-TACCCCC;

DDX18: F- TGACTCACCACGTGCATACC, R- TGCATATG-GTCCAGCAGACG;

DDX41: F- CAGGAGGAACGGACTAAGGC, R- CGGCCAATCCG-GTGTACATA;

TAF15: F- GATCAGCGCAACCGACCATA, R- CAAGAAGAGGC-CACGAGGAA.

35S pulse/chase

For ^{35}S pulse experiments, HEK293T cells were labelled with methionine ^{35}S and cysteine ^{35}S for different amounts of time (10–60 min). After washing cells were lysed in immunoprecipitation lysis buffer (50 mM Tris–HCl pH 8, 150 mM NaClm 1 mM EDTA, 1% Nonidet P-40, 1% SDS, supplemented with protease inhibitor cocktail). HTT^{Q43}GFP was pulled down using magnetic GFP-trap beads (ChromoTek). Pull downs were loaded on SDS gels and analysed using western blot or AR. Autograph intensity reflects the amount of HTT^{Q43}GFP containing ^{35}S in pull down or whole cell extraction. Total amount of HTT^{Q43}GFP were measured by western blot using anti-GFP antibody. α-tubulin was used as loading control.

For ^{35}S pulse chase experiments, HEK293T cells were transfected with HTT^{Q43}GFP, with or without FOXO1. Cells were labelled with methionine^{35}S and cysteine^{35}S for 1.5 h. After washing, cells were incubated in normal cultural media for different amounts of time. Cells were lysed, HTT^{Q43}GFP was pulled down and analysis was done as described for the ^{35}S pulse experiments by GFP-trap. For quantitative analysis, autograph intensity was normalized by loading control or total pulled down GFP. Then, all the later time points were normalized against 0 h.

The data of the control [empty vector (EV)] of both the pulse and pulse chase experiments have been published before as the experiments to determine the stability and synthesis of HTT^{Q43}GFP after expression of IGF2 or FOXO1 have been conducted together (10).

RNA pull down-MS

HEK293T cells were transfected with or without FOXO1 using Polyfect (Qiagen). Cells were lysed 48 h post-transfection in Buffer D (20 mM Tris pH7,9, 20% glycerol, 0,1MKCl, 0,2 mM EDTA, 0,5 mM DTT, protease inhibitor, RNase inhibitor) by sonication. Biotinylated HTT^{CAG47} mRNA was generated by PCR-amplification of HTT-exon1 using primers with a T7 site in the forward primer (CCAAGCTTCTAATACGACTCAC-TATAGGGAGAATGGCGGACCCTGGAAAAGCTCATGAAGG and GGTCGGTGCAGCGGCTCCTCAGC) and *in vitro* transcription using the T7 RiboMAX Kit (Promega). Purified transcripts were then coated onto Streptavidin–Agarose beads (SIGMA) and incubated with cell lysates. After washing the beads with Buffer D, RNA-bound proteins were analysed by mass spec at the UMCG. Mass spec analysis was done on three biological repeats.

Bioinformatics

GO-term enrichment analysis was performed using DAVID 6.8. Fold enrichment and P-value were corrected by the Benjamini methods.

CRISRPi

CRISRPi was following the protocol from Matthew H Larson, 2013 (39). Briefly, dCas9-KRAB (#71237) and sgRNA (#44248) were obtained from Addgene. dCas9-KRAB was cloned into mammalian expression vector pcDNA 3.1. sgRNA was designed by CRISPR-ERA v1.2 (http://crispr-era.stanford.edu/) following the standard protocol. sgRNAs sequences are listed below:

    STAU1: GGCGGCTGCCGCGTCTCTCT
    IGF2BP3: GGAAGACTGGTGGATGCGTT
    FUS: GCGTCGGTACTCAGCGGTGT
    DDX18: GCCTTATTCTAGGCACTTGT
    DDX41: GACTGGCGTGTGCTTGCAGC
    TAF15: GCTTTCGTATTCGTTGTTCT

Statistical analysis

Results were statistically compared using the Student's t test was performed for unpaired or paired groups or 1-way analysis of variance with the Bonferroni correction for multiple groups. A P-value of < 0.05 was considered significant (*$P < 0.05$, **$P < 0.01$, ***$P < 0.001$).

Supplementary Material

Supplementary Material is available at *HMG* online.

Acknowledgement

Conflict of Interest statement. None declared.

Abbreviations

AR, Autoradiography, DBD, DNA binding domain, EV, Empty vector, FTA, Filter trap assay, HSPB, Small heat shock protein, PolyQ, Polyglutamine, TAD, Transcription activation domain, UPS, Ubiquitin–proteasome system, WT, wild-type.

References

1. Kuiper, E.F.E., de Mattos, E.P., Jardim, L.B. *et al.* (2017) Chaperones in polyglutamine aggregation: beyond the Q-stretch. *Front. Neurosci.*, **11**, 45.
2. Lieberman, A.P., Shakkottai, V.G. and Albin, R.L. (2019) Polyglutamine repeats in neurodegenerative diseases. *Annu. Rev. Pathol. Mech. Dis.*, **14**, 1–27.
3. Balch, W.E., Morimoto, R.I., Dillin, A. *et al.* (2008) Adapting proteostasis for disease intervention. *Science (80-.).*, **319**, 916–919.
4. Kampinga, H.H. and Bergink, S. (2016) Heat shock proteins as potential targets for protective strategies in neurodegeneration. *Lancet Neurol.*, **15**, 748–759.
5. Weber, J.J., Sowa, A.S., Binder, T. *et al.* (2014) From pathways to targets: understanding the mechanisms behind polyglutamine disease. From pathways to targets: understanding the mechanisms behind polyglutamine disease. *Biomed. Res. Int.*, **2014**, 701758.
6. Kim, Y.E., Hipp, M.S., Bracher, A. *et al.* (2013) Molecular chaperone functions in protein folding and proteostasis. *Annu. Rev. Biochem.*, **82**, 323–355.
7. de Mezer, M., Wojciechowska, M., Napierala, M. *et al.* (2011) Mutant CAG repeats of Huntingtin transcript fold into hairpins, form nuclear foci and are targets for RNA interference. *Nucleic Acids Res.*, **39**, 3852–3863.
8. Nalavade, R., Griesche, N., Ryan, D.P. *et al.* (2013) Mechanisms of RNA-induced toxicity in CAG repeat disorders. *Cell Death Dis.*, **4**, e752–e752.
9. Buijsen, R.A.M., Toonen, L.J.A., Gardiner, S.L. *et al.* (2019) Genetics, mechanisms, and therapeutic progress in polyglutamine spinocerebellar ataxias. *Neurotherapeutics*, **16**, 263–286.
10. García-Huerta, P., Troncoso-Escudero, P., Wu, D. *et al.* (2020) Insulin-like growth factor 2 (IGF2) protects against Huntington's disease through the extracellular disposal of protein aggregates. *Acta Neuropathol.*, **140**, 737–764.
11. Pennuto, M., Pandey, U.B. and Polanco, M.J. (2020) Insulin-like growth factor 1 signaling in motor neuron and polyglutamine diseases: from molecular pathogenesis to therapeutic perspectives. Insulin-like growth factor 1 signaling

in motor neuron and polyglutamine diseases: from molecular pathogenesis to therapeutic perspectives. *Front. Neuroendocrinol.*, **57**, 100821.

12. Thiruvalluvan, A., de Mattos, E.P., Brunsting, J.F. *et al.* (2020) DNAJB6, a key factor in neuronal sensitivity to Amyloidogenesis. *Mol. Cell.*

13. Cohen, E. and Dillin, A. (2008) The insulin paradox: aging, proteotoxicity and neurodegeneration. *Nat. Rev. Neurosci.*, **9**, 759–767.

14. Cunha-Santos, J., Duarte-Neves, J., Carmona, V. *et al.* (2016) Caloric restriction blocks neuropathology and motor deficits in Machado–Joseph disease mouse models through SIRT1 pathway. *Nat. Commun.*, **7**, 11445.

15. Johnson, T. (1990) Increased life-span of age-1 mutants in *Caenorhabditis elegans* and lower Gompertz rate of aging. *Science (80-.)*, **249**, 908–912.

16. Lalić, N.M., Marić, J., Svetel, M. *et al.* (2008) Glucose homeostasis in Huntington disease. *Arch. Neurol.*, **65**, 476.

17. Moll, L., Ben-Gedalya, T., Reuveni, H. *et al.* (2016) The inhibition of IGF-1 signaling promotes proteostasis by enhancing protein aggregation and deposition. *FASEB J.*, **30**, 1656–1669.

18. Morley, J.F., Brignull, H.R., Weyers, J.J. *et al.* (2002) The threshold for polyglutamine-expansion protein aggregation and cellular toxicity is dynamic and influenced by aging in *Caenorhabditis elegans*. *Proc. Natl. Acad. Sci.*, **99**, 10417–10422.

19. Saute, J.A.M., da Silva, A.C.F., Muller, A.P. *et al.* (2011) Serum insulin-like system alterations in patients with spinocerebellar ataxia type 3. *Mov. Disord.*, **26**, 731–735.

20. Hsu, A.-L. (2003) Regulation of aging and age-related disease by DAF-16 and heat-shock factor. *Science (80-.)*, **300**, 1142–1145.

21. Walker, G.A. and Lithgow, G.J. (2003) Lifespan extension in C. elegans by a molecular chaperone dependent upon insulin-like signals. *Aging Cell*, **2**, 131–139.

22. van Waarde-Verhagen, M.A.W.H. and Kampinga, H.H. (2018) Measurement of chaperone-mediated effects on Polyglutamine protein aggregation by the filter trap assay. *Methods Mol. Biol.*, 59–74.

23. Vidal, R.L., Figueroa, A., Court, F.A. *et al.* (2012) Targeting the UPR transcription factor XBP1 protects against Huntington's disease through the regulation of FoxO1 and autophagy. *Hum. Mol. Genet.*, **21**, 2245–2262.

24. Vos, M.J., Zijlstra, M.P., Kanon, B. *et al.* (2010) HSPB7 is the most potent polyQ aggregation suppressor within the HSPB family of molecular chaperones. *Hum. Mol. Genet.*, **19**, 4677–4693.

25. Wu, D., Vonk, J.J., Salles, F. *et al.* (2019) The N terminus of the small heat shock protein HSPB7 drives its polyQ aggregation-suppressing activity. *J. Biol. Chem.*, **294**, 9985–9994.

26. Papaevgeniou, N. and Chondrogianni, N. (2014) The ubiquitin proteasome system in *Caenorhabditis elegans* and its regulation. *Redox Biol.*, **2**, 333–347.

27. Zečić, A. and Braeckman, B.P. (2020) DAF-16/FoxO in *Caenorhabditis elegans* and its role in metabolic remodeling. *Cell.*

28. Zhao, Y., Yang, J., Liao, W. *et al.* (2010) Cytosolic FoxO1 is essential for the induction of autophagy and tumour suppressor activity. *Nat. Cell Biol.*, **12**, 665–675.

29. Ravikumar, B. (2002) Aggregate-prone proteins with polyglutamine and polyalanine expansions are degraded by autophagy. *Hum. Mol. Genet.*, **11**, 1107–1117.

30. Kuma, A., Hatano, M., Matsui, M. *et al.* (2004) The role of autophagy during the early neonatal starvation period. *Nature*, **432**, 1032–1036.

31. Minoia, M., Boncoraglio, A., Vinet, J. *et al.* (2014) BAG3 induces the sequestration of proteasomal clients into cytoplasmic puncta. *Autophagy*, **10**, 1603–1621.

32. Yang, J., Hao, X., Cao, X. *et al.* (2016) Spatial sequestration and detoxification of Huntingtin by the ribosome quality control complex. *elife*, **5**.

33. Conlon, E.G. and Manley, J.L. (2017) RNA-binding proteins in neurodegeneration: mechanisms in aggregate. RNA-binding proteins in neurodegeneration: mechanisms in aggregate. *Genes Dev.*, **31**, 1509–1528.

34. Krauß, S., Griesche, N., Jastrzebska, E. *et al.* (2013) Translation of HTT mRNA with expanded CAG repeats is regulated by the MID1–PP2A protein complex. *Nat. Commun.*, **4**, 1511.

35. McLaughlin, B.A., Spencer, C. and Eberwine, J. (1996) CAG trinucleotide RNA repeats interact with RNA-binding proteins. *Am. J. Hum. Genet.*, **59**, 561–569.

36. Schilling, J., Broemer, M., Atanassov, I. *et al.* (2019) Deregulated splicing is a major mechanism of RNA-induced toxicity in Huntington's disease. *J. Mol. Biol.*, **431**, 1869–1877.

37. Hubstenberger, A., Courel, M., Bénard, M. *et al.* (2017) P-body purification reveals the condensation of repressed mRNA regulons. *Mol. Cell*, **68**, 144, e5–157.

38. Youn, J.-Y., Dyakov, B.J.A., Zhang, J. *et al.* (2019) Properties of stress granule and P-body proteomes. *Mol. Cell*, **76**, 286–294.

39. Larson, M.H., Gilbert, L.A., Wang, X. *et al.* (2013) CRISPR interference (CRISPRi) for sequence-specific control of gene expression. *Nat. Protoc.*, **8**, 2180–2196.

40. Mancarella, C. and Scotlandi, K. (2020) IGF2BP3 from physiology to cancer: novel discoveries, unsolved issues, and future perspectives. *Front. Cell Dev. Biol.*, **7**, 363.

41. Ennajdaoui, H., Howard, J.M., Sterne-Weiler, T. *et al.* (2016) IGF2BP3 modulates the interaction of invasion-associated transcripts with RISC. *Cell Rep.*, **15**, 1876–1883.

42. Treiber, T., Treiber, N. and Meister, G. (2019) Regulation of microRNA biogenesis and its crosstalk with other cellular pathways. *Nat. Rev. Mol. Cell Biol.*, **20**, 5–20.

43. Aalto, A.P., Nicastro, I.A., Broughton, J.P. *et al.* (2018) Opposing roles of microRNA Argonautes during *Caenorhabditis elegans* aging. *PLoS Genet.*, **14**, e1007379.

44. Barker, R.A., Fujimaki, M., Rogers, P. *et al.* (2020) Huntingtin-lowering strategies for Huntington's disease. *Expert Opin. Investig. Drugs*, **29**, 1125–1132.

45. Song, H.M., Song, J.L., Li, D.F. *et al.* (2015) Inhibition of FOXO1 by small interfering RNA enhances proliferation and inhibits apoptosis of papillary thyroid carcinoma cells via Akt/FOXO1/Bim pathway. *Onco. Targets. Ther.*, **8**, 3565–73.

46. Hageman, J., Rujano, M.A., van Waarde, M.A.W.H.W.H. *et al.* (2010) A DNAJB chaperone subfamily with HDAC-dependent activities suppresses toxic protein aggregation. *Mol. Cell.*, **37**, 355–69.

47. Meister-Broekema, M., Freilich, R., Jagadeesan, C. *et al.* (2018) Myopathy associated BAG3 mutations lead to protein aggregation by stalling Hsp70 networks. *Nat. Commun.*, **9**, 5342.

48. Kakkar, V., Månsson, C., de Mattos, E.P. *et al.* (2016) The S/T-rich motif in the DNAJB6 chaperone delays Polyglutamine aggregation and the onset of disease in a mouse model. *Mol. Cell*, **62**, 272–283.